





Influence of the magnetovolume effect on the transient reflectivity of MnSiJ. Kalin ^{*}, S. Sievers , H. W. Schumacher, H. Füsler , and M. Bieler *Physikalisch-Technische Bundesanstalt, 38116 Braunschweig, Germany*A. Bauer *Physik-Department, Technische Universität München, 85748 Garching, Germany
and Zentrum für QuantumEngineering (ZQE), Technische Universität München, 85748 Garching, Germany*

C. Pfleiderer

*Physik-Department, Technische Universität München, 85748 Garching, Germany;
Zentrum für QuantumEngineering (ZQE), Technische Universität München, 85748 Garching, Germany;
Munich Center for Quantum Science and Technology (MCQST), Technische Universität München, 85748 Garching, Germany;
and Heinz Maier-Leibnitz Zentrum (MLZ), Technische Universität München, 85748 Garching, Germany*

(Received 3 February 2024; accepted 28 May 2024; published 11 July 2024)

The magnetovolume effect is a well established yet frequently overlooked phenomenon in magnetic materials that may affect a wide range of physical properties. Our study explores the influence of the magnetovolume effect on the transient reflectivity of MnSi, a well-known chiral magnet with strong magnetoelastic coupling. We observe a unipolar reflectivity transient in the paramagnetic phase, contrasting with a bipolar response in phases with magnetic long-range order. Comparing our findings with thermal expansion from literature, we establish that the bipolar response originates in the magnetovolume effect which dominates the thermal expansion and influences the optical reflectivity. Our results highlight not only that the magnetovolume effect must be considered when discussing transient reflectivity measurements of magnetic materials but also that such measurements permit to study the characteristic time scales of the magnetovolume effect itself, contributing to a deeper understanding of this often-neglected phenomenon.

DOI: [10.1103/PhysRevB.110.014415](https://doi.org/10.1103/PhysRevB.110.014415)**I. INTRODUCTION**

The interaction of femtosecond laser pulses with magnetic materials gives rise to intriguing phenomena, such as ultrafast demagnetization [1,2], all-optical switching [3], and excitation of collective spin dynamics [4]. To effectively model these effects in micromagnetic simulations and investigate the underlying physical processes, knowledge of the transient temperature response of the material after thermal excitation represents a key prerequisite [5,6]. The standard technique for determining the transient temperature responses is based on time-resolved transient reflectivity measurements, probing the change of the optical reflectivity ΔR due to thermal laser excitation.

In the typical framework of transient reflectivity [7–12], the reflectivity of a metal is used as a thermometer, as ΔR is assumed to be proportional to the transient electron [7,11,13] and lattice [8,12] temperature. The evolution of these temperatures as a function of time is described by the two-temperature model [14], which treats the electronic and lattice systems as coupled heat baths. Thus, the laser-induced changes of the optical reflectivity are commonly described as the result of two contributions [9]: (i) thermal alteration of the electron density

distribution [7,10] and (ii) excitation of phonons associated with thermal expansion [8,12,13].

However, in magnetic materials additional effects may impact the transient reflectivity due to the quenching of magnetic order upon femtosecond laser excitation, challenging the standard picture of transient reflectivity. Perhaps most notably, the magnetovolume effect, i.e., the volume change arising from a change of the magnetic order [15] due to magnetoelastic coupling, gives rise to modifications of the electron interband and intraband transition rates at optical frequencies and thus to changes of the optical reflectivity. The magnetovolume effect was extensively studied in thermal equilibrium [15–20], but its impact on ultrafast timescales [21–23] and its consequences on optical reflectivity is less explored.

In this article, we investigate the influence of long-range magnetic order and the magnetovolume effect on the transient reflectivity of the archetypical chiral magnet MnSi in optical pump-probe experiments. We confirm the alteration of magnetic order upon laser excitation in time-resolved magneto-optical Kerr effect (TR-MOKE) measurements and compare the magnetization dynamics to the transient reflectivity. Our study reveals, that the temporal evolution of the transient reflectivity changes drastically from a unipolar behavior in the paramagnetic phase to a bipolar signal in the states with long-range magnetic order. By a comparison of the transient reflectivity and thermal expansion we show that

^{*}Contact author: jantje.kalin@ptb.de

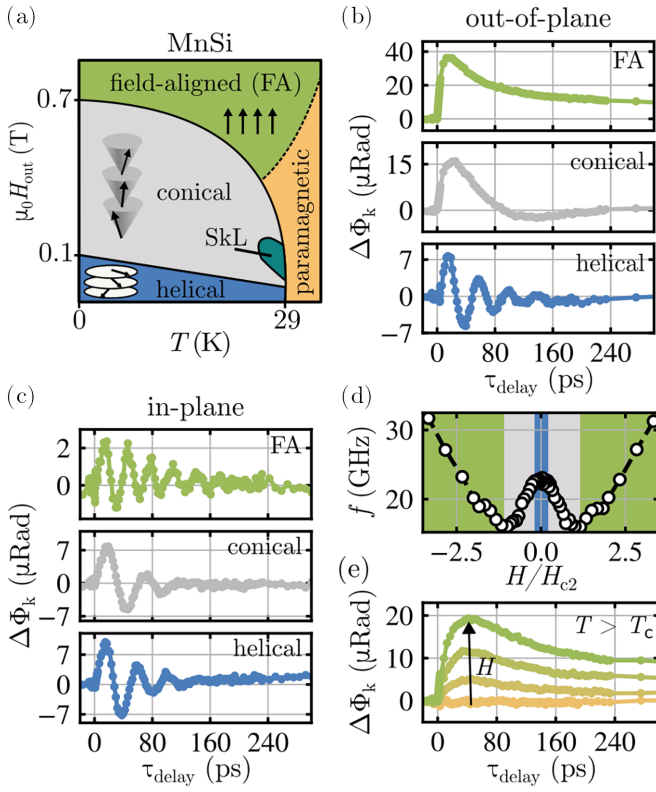


FIG. 1. (a) Schematic magnetic phase diagram of MnSi for magnetic fields along $\langle 110 \rangle$. The critical fields $\mu_0 H_{c1} \approx 0.1$ T and $\mu_0 H_{c2} \approx 0.7$ T for magnetic field transitions as well as the critical temperature $T_c = 29$ K are indicated. (b) and (c) Typical out-of-plane (b) and in-plane (c) TR-MOKE signals in the field-aligned (FA), conical, and helical phases at 10 K. (d) Dispersion extracted from the in-plane TR-MOKE signals at 10 K indicating the characteristic spin modes of the helical, conical, and field-aligned phase. (e) Out-of-plane TR-MOKE signal of the paramagnetic phase for various magnetic fields [0, 0.2, 0.5, 1.0] T at 39 K.

the bipolar signal is caused by the magnetovolume effect dominating the thermal expansion. These results contribute to an improved understanding of transient reflectivity of materials exhibiting magnetovolume effect, which is the case for most magnetic materials close to phase transitions. Further, this study shows how to accurately determine the transient temperature response of these materials.

II. THE BULK CHIRAL MAGNET MnSi

We focus on the bulk chiral magnet MnSi, owing to its pronounced magnetovolume effect [17–20,24] and its magnetic phase diagram [25], depicted in Fig. 1(a), which permits to study the transient reflectivity of different magnetic states. At high temperatures, MnSi is a paramagnet. As the temperature is lowered beneath the critical temperature $T_c = 29$ K, long-range magnetic order emerges. In this temperature regime, MnSi shows a helical phase for magnetic fields smaller than a critical field value H_{c1} . This phase is characterized by long-wavelength spin spirals, which are aligned along the magnetically easy axes $\langle 111 \rangle$ of the lattice. For magnetic fields above H_{c1} , the spins tilt toward the magnetic field

direction, resulting in a conical phase. Finally, for magnetic fields larger than the critical field H_{c2} , the spins align collinearly in the field-aligned phase. Just below the critical temperature in a small regime in the magnetic phase diagram, MnSi shows a skyrmion lattice state with a spin swirling structure [26].

MnSi exhibits a significant magnetovolume effect [17–20,24], driven by magnetoelastic coupling. Due to that the sample's volume, changes in response to variations in magnetic field and temperature, as the magnetic order varies with these parameters. Via the temperature dependence, the magnetovolume effect influences the thermal expansion and leads to an anomalous behavior. For $T \gg T_c$ and at low magnetic fields in the paramagnetic phase, MnSi shows an ordinary positive thermal expansion caused by the excitation of phonons and electrons, leading to a contraction of the lattice upon cooling. In contrast, the lattice of MnSi expands upon cooling for temperatures below and in proximity to T_c and shows a negative thermal expansion. This behavior is explained by the magnetovolume effect surpassing the positive thermal expansion caused by phonons and electrons. Thereby, the magnetovolume effect is largest close to the phase transition at T_c . At high magnetic fields above T_c , where the magnetic moments orient along the direction of the field, the magnetovolume effect and a negative thermal expansion is again observed [24].

III. EXPERIMENTAL SETUP FOR TRANSIENT REFLECTIVITY AND TR-MOKE MEASUREMENTS

In this study, TR-MOKE and transient reflectivity measurements were performed simultaneously in a femtosecond pump-probe experiment. Laser pulses of about 150 fs duration with a center wavelength of 800 nm and a repetition rate of 76 MHz are generated by a Ti:Sapphire oscillator. The linearly polarized laser light is split into a pump and probe beam. The pump beam, which hits the sample under nearly normal incidence with a fluence of $2 \mu\text{Jcm}^{-2}$, thermally excites the MnSi sample ($2 \times 2 \times 0.5 \text{ mm}^3$) by laser heating. In addition to steady-state heating, which is around 4 K and accounted for when estimating the base temperature, laser heating with the femtosecond laser pulses introduces a temperature increase on the ultrafast timescale. At 10 K and for the used laser fluence, laser heating in our experiment [27] leads to a maximum change in electron, lattice, and spin temperature of $\Delta T_{e,\text{max}} = 18$ K, $\Delta T_{L,\text{max}} = 14$ K, and $\Delta T_{s,\text{max}} = (15 \pm 3)$ K, respectively. The transient temperature increase modulates the optical properties of the sample on an ultrafast timescale and excites spin dynamics. By analyzing the probe beam after nearly normal reflection from the sample surface, the transient reflectivity is inferred from the thermally induced amplitude changes of the reflectivity $\Delta R/R$. In contrast, in TR-MOKE the change of the polarization state of the reflected probe beam is measured and quantified by the variations in the Kerr angle $\Delta\phi_k$. Due to the small incidence angle of the probe beam, $\Delta\phi_k$ is mainly sensitive to the changes of the out-of-plane magnetization component. In order to enhance the detection sensitivity, the amplitude of the pump beam is modulated at a frequency of 3 kHz by an optical chopper. The time-resolved measurements are achieved by modifying the time delay τ_{delay}

between the pump and probe beams. This enables the detection of optical changes versus time with subpicosecond resolution. A cryostat with a superconducting magnet is utilized to control the applied magnetic field and sample temperature. We apply magnetic fields which point in and out of the sample plane in the $\langle 110 \rangle$ crystal direction and refer to them as in-plane and out-of-plane measurements. The in-plane and out-of-plane TR-MOKE signals reflect thermally induced changes in magnetization perpendicular ($dm/dt \perp H$) and parallel ($dm/dt \parallel H$) to the applied magnetic field, respectively.

IV. LASER-EXCITED SPIN DYNAMICS OF MnSi

In Figs. 1(b) and 1(c), in- and out-of-plane TR-MOKE signals are presented for the field-aligned (FA), conical, helical, and paramagnetic phase. Following optical pump beam excitation at zero time, we observe a rapid rise in the TR-MOKE signal indicating thermal alteration of magnetic order by laser heating [2]. Subsequently, the signal decreases as the magnetic state recovers. In the FA and conical phase, recovery manifests as collective precessional dynamics observed in the in-plane TR-MOKE measurements in Fig. 1(c). As collective dynamics predominantly occur in the sample plane perpendicular to the applied magnetic field for the FA and conical phase, the out-of-plane TR-MOKE signals exhibit a monotonous decay, consistent with prior studies on chiral magnets [28,29]. In the conical phase, the out-of-plane TR-MOKE signal decays on a much faster timescale compared to the FA phase, with a small overshoot to negative values. Precessional remagnetization behavior is observed for the helical phase in both the in- and out-of-plane TR-MOKE signals, attributed to the alignment of the helical phase with the direction of magnetically easy axes. An analysis of the oscillation frequency as a function of the applied field shows that the observed precessional dynamics exhibit the characteristic dispersion of the spin eigenmodes of the different magnetic phases of MnSi [30], as illustrated in Fig. 1(d). For the paramagnetic phase, only the out-of-plane TR-MOKE signal for $B > 0$ T is nonzero. Here, we observe an increase of $\Delta\phi_k$ with the applied magnetic field, see Fig. 1(e), indicating field-induced spin alignment. Overall, the TR-MOKE measurements indicate a thermally induced alteration of the magnetic order by laser heating. Thereby, the different magnetic phases of MnSi can be unambiguously identified using characteristic signatures within the TR-MOKE signal.

V. TRANSIENT REFLECTIVITY OF MnSi

Next, we study the transient reflectivity of the different magnetic phases of MnSi. In Figs. 2(a) and 2(b) the transient reflectivity at zero magnetic field well above and below T_c , i.e., in the paramagnetic and helical phase, is shown. For the paramagnetic phase, we observe a rapid increase of $\Delta R/R$ upon application of the pump pulse at $t = 0$ ps. After this transient reflectivity shows an exponential decay as the signal gradually returns to its initial state, resulting in a unipolar transient reflectivity signal. In contrast, in the helical phase the rapid increase of the reflectivity signal is followed by a zero crossing and a large negative transient, leading to a bipolar temporal evolution of the thermally induced reflectivity

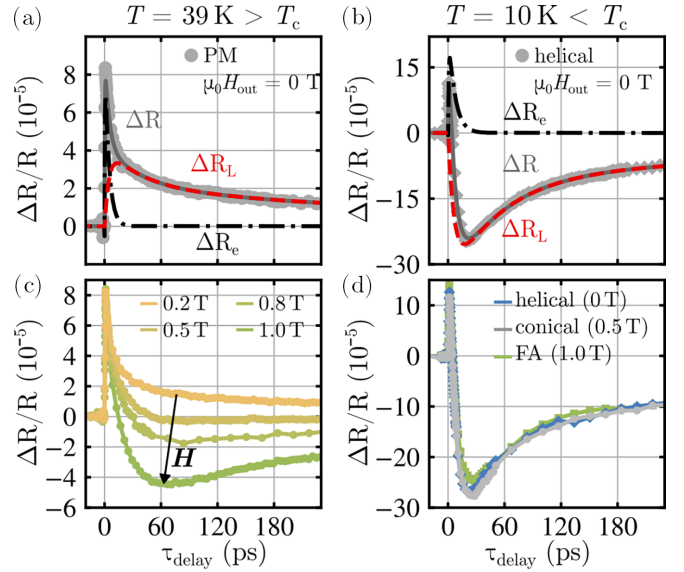


FIG. 2. Transient reflectivity of the different magnetic states of MnSi. (a) Paramagnetic phase at $T = 39$ K and $\mu_0 H_{\text{out}} = 0$ T shown with fit to the experimental data using the model of Eq. (1). (b) Helical phase at $T = 10$ K and $\mu_0 H_{\text{out}} = 0$ T shown with fit to the experimental data using the model of Eq. (1). (c) Paramagnetic phase at $T = 39$ K $> T_c$ and various magnetic fields, which point out of the sample plane along the $\langle 110 \rangle$ direction. (d) States with long-range magnetic order at low temperatures $T = 10$ K, namely, helical phase at 0 T, conical phase at 0.5 T, and field-aligned phase at 1.0 T. The magnetic field is pointing out of the sample plane along the $\langle 110 \rangle$ direction.

change [31]. Thus, the transient reflectivity at zero magnetic field shows a different behavior well above and below the critical temperature.

In Figs. 2(c) and 2(d), we show transient reflectivity measurements for different magnetic fields for $T \gg T_c$ and $T < T_c$. Well above T_c , we observe a transition from the unipolar transient to the bipolar signal with increasing magnetic field. Here, the applied magnetic field forces an alignment of magnetic moments in the paramagnetic phase. In the magnetically ordered states below T_c , however, we observe independent of the applied magnetic field and magnetic configuration a bipolar signal, as shown by the comparison of the transient reflectivity of the helical, conical, and field-aligned phase in Fig. 2(d). Accordingly, the bipolar reflectivity signal occurs independently of the exact magnetic state. Thereby, the bipolar reflectivity transient is observed independent of the magnetic field polarity and direction, i.e., out-of- and in-plane magnetic fields, as well as the polarization of the probe beam (not shown). Together with the absence of contributions attributed to precessional dynamics in the reflectivity transient, especially at 0 T in the helical phase, this rules out magneto-optical effect as cause of the bipolar reflectivity. At the same time it confirms that the TR-MOKE measurements in Fig. 1 represent the magnetization dynamics and not the change of reflectivity [32].

To analyze the transient reflectivity of MnSi further, we apply the conventional phenomenological model for metals and assume that the reflectivity is proportional to the electron

and lattice temperature [9,12]. Thus, $\Delta R/R$ is a superposition of an electronic $\Delta R_e/R$ and a lattice reflectivity transient $\Delta R_L/R$:

$$\begin{aligned} \frac{\Delta R(\tau_{\text{delay}})}{R} &= \frac{\Delta R_e(\tau_{\text{delay}})}{R} + \frac{\Delta R_L(\tau_{\text{delay}})}{R} \\ &= A \cdot \Delta T_e(\tau_{\text{delay}}) + B \cdot \Delta T_L(\tau_{\text{delay}}). \end{aligned} \quad (1)$$

The term $\Delta R_e/R$ describes the reflectivity change due to the increase of the electron temperature T_e by laser heating and accounts for the laser-excited electrons and their thermalization. The second term $\Delta R_L/R$ models the transient reflectivity contribution stemming from an increase in lattice temperature T_L and covers the change of the optical reflectivity due to thermal expansion of the lattice. Thereby, A and B describe the proportionality of $\Delta R_e/R$ and $\Delta R_L/R$ to the change in electron and lattice temperature, respectively. Both A and B can be positive or negative depending on how the optical transition rates and thus the optical reflectivity are modulated by the change in the electron and lattice distribution [12]. The key components of the transient electron ΔT_e and lattice ΔT_L temperature are exponential rise and decay functions. They are given by

$$\begin{aligned} \Delta T_e(\tau_{\text{delay}}) &= \Delta T_{e,\text{max}} \cdot [1 - \exp(-\tau_{\text{delay}}/\tau_{ee})] \cdot \\ &\quad \times \exp(-\tau_{\text{delay}}/\tau_{eL}) \cdot \Theta(\tau), \end{aligned} \quad (2)$$

$$\begin{aligned} \Delta T_L(\tau_{\text{delay}}) &= \Delta T_{L,\text{max}} \cdot [1 - \exp(-\tau_{\text{delay}}/\tau_{eL})] \cdot [\beta_1 \cdot \\ &\quad \times \exp(-\tau_{\text{delay}}/\tau_{th}) \\ &\quad + \beta_2 \cdot \exp(-\tau_{\text{delay}}/\tau_{th,2})] \cdot \Theta(\tau). \end{aligned} \quad (3)$$

Here, $\Delta T_{e,\text{max}}$ and $\Delta T_{L,\text{max}}$ are the maximum change of the electron and lattice temperature due to laser heating, which we estimate in a framework based on the 3T model [27]. The time constant τ_{ee} describes the rise time of the electron reflectivity transient, τ_{eL} is the electron-lattice thermalization, τ_{th} is the diffusion time constant and $\tau_{th,2}$ is a second decay time of ΔR_L . The τ_{ee} is determined by the time the electron system needs to equilibrate in energy and form a Fermi-Dirac distribution [12]. Further, τ_{ee} is influenced by the laser pulse width, because it determines the time to deposit the laser energy into the electron system [12]. The second decay time $\tau_{th,2}$ accounts for the double exponential decay of the negative transient observed in Figs. 2(b)–2(d). The parameters β_i represent the amplitudes of the exponential decay terms of ΔT_L , ranging between zero and one. The term $\Theta(\tau)$ is an error function and describes the finite width of the probe pulse and the start of excitation at $t = 0$. In the analysis, we assume that the thermalization of nonthermal electrons and lattice is comparable or smaller than the laser pulse width. Therefore, we do not consider nonthermal dynamics of electrons and the lattice [33].

In Figs. 2(a) and 2(b) fits of the phenomenological model to the unipolar and bipolar reflectivity transient are shown. In both cases, we obtain excellent agreement of model and the data. Remarkably, the electronic $\Delta R_e/R$ and lattice reflectivity transient $\Delta R_L/R$ are both positive for the unipolar signal, while $\Delta R_L/R$ is negative in the case of the bipolar transient. The transition from a unipolar to a bipolar reflectivity transient can therefore be related to a change in polarity of $\Delta R_L/R$.

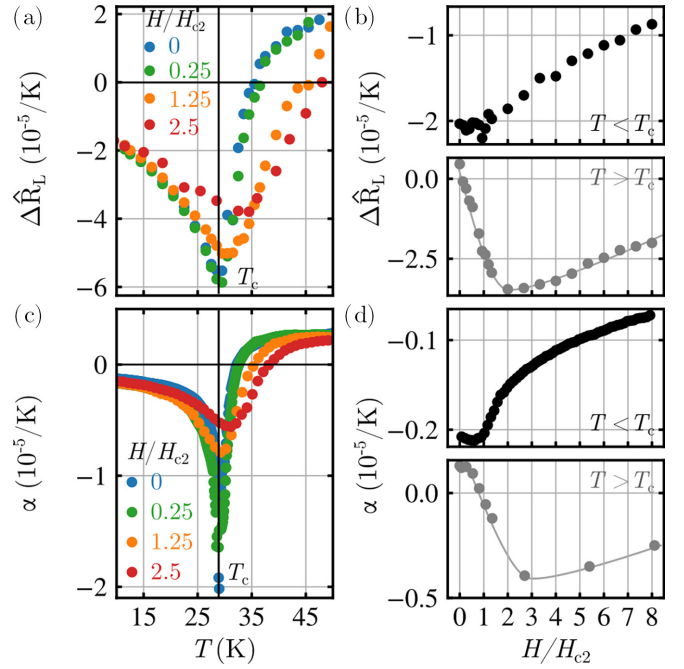


FIG. 3. (a) Temperature dependence of the amplitude of the lattice reflectivity transient $\Delta \hat{R}_L$ at four different magnetic field values. (b) Magnetic field dependence of $\Delta \hat{R}_L$ below (10 K, top) and above (35 K, bottom) the critical temperature. (c) Coefficient of linear thermal expansion α of MnSi from Ref. [19] as a function of temperature for four different magnetic field values. (d) Magnetic field dependence of α at 10 K $< T_c$ from Ref. [20] (top) and at 35 K $> T_c$ from Ref. [19].

We further investigate the polarity of $\Delta R_L/R$ by analyzing its amplitude as a function of temperature and applied magnetic field. According to Eqs. (1)–(3) the amplitude of $\Delta R_L/R$ is equal to $B \cdot \Delta T_{L,\text{max}}$. We exclude the temperature dependence of $\Delta T_{L,\text{max}}$ [27] in our analysis by considering $\Delta \hat{R}_L = B$ in the following. As illustrated in Fig. 3(a) for various magnetic fields, the amplitude of the transient reflectivity $\Delta \hat{R}_L$ changes sign with temperature. For $T < T_c$, $\Delta \hat{R}_L$ is negative and decreases at higher temperatures. At T_c , $\Delta \hat{R}_L$ shows its minimum and increases versus temperature until it turns positive. Subsequently, the positive $\Delta \hat{R}_L$ rises with temperature. Further, we observe a shift of the minimum $\Delta \hat{R}_L$ to higher temperatures with increasing magnetic field. At the same time, zero crossing of $\Delta \hat{R}_L$ occurs for larger temperatures upon increase of the magnetic field.

The magnetic field dependence of $\Delta \hat{R}_L$ is presented in Fig. 3(b). For $T < T_c$, $\Delta \hat{R}_L$ varies only slightly with magnetic field up to H_{c2} and increases for higher values in the field-aligned phase [see the upper panel in Fig. 3(b)]. Thereby, it remains negative in the entire magnetic field range. At $T > T_c$, we observe a different behavior of the lattice transient reflectivity, as shown in the lower panel in Fig. 3(b) for 35 K. Here, $\Delta \hat{R}_L$ first decreases for increasing magnetic field and then increases again, possibly due to a transition from the paramagnetic to the field-aligned phase. Thereby, the sign of $\Delta \hat{R}_L$ changes from positive to negative for small magnetic fields at $T > 35$ K, as shown as well in Fig. 3(a). Overall,

we observe a different magnetic field dependence of $\Delta\hat{R}_L$ for $T < T_c$ and $T > T_c$.

VI. COMPARISON OF TRANSIENT REFLECTIVITY AND THERMAL EXPANSION

According to the conventional model applied above, the lattice contribution to transient reflectivity is due to the changes in the optical properties caused by thermal expansion of the lattice [9,12,13]. With the help of the amplitude analysis of $\Delta R_L/R$, we can compare the transient reflectivity measurements with thermal expansion data. For the comparison, we take the coefficient of linear thermal expansion $\alpha = (1/L_0)dL/dT$ measured with a capacity dilatometer on a comparable MnSi sample from Refs. [19] and [20] as a measure of thermal expansion. Here, L_0 is the sample length at 300 K and dL/dT is the change of sample length with temperature. For the data from Ref. [20] we approximate α by $(1/L_0)(\Delta L(T_2) - \Delta L(T_1))/(T_2 - T_1)$ using measurements of the linear thermal expansion $\Delta L/L_0$ at different temperatures.

In Figs. 3(c) and 3(d) the coefficient of linear thermal expansion α as a function of temperature and applied magnetic field is shown. Like the amplitude of the lattice reflectivity transient, α peaks at T_c and changes sign with increasing temperature. Note, that the sharp peak at T_c seen in α for $H < H_{c2}$ is not observed for $\Delta\hat{R}_L$, most likely due to larger temperature increases from laser heating and the averaging of the temperature-dependent signal in the transient reflectivity data. Further, α has a very similar dependence on the magnetic field as $\Delta\hat{R}_L$, since it shows the distinct variations with field above and below T_c . The similarity of $\Delta\hat{R}_L$ and α indicates that the shift in polarity of $\Delta R_L/R$ can be explained by the temperature and magnetic field dependence of thermal expansion. It's noteworthy that specific heat, thermal expansion, and the temperature derivative of resistivity exhibit a unified temperature dependence [24]. However, the sign change only observed for the thermal expansion is the driving force for the polarity reversal of $\Delta R_L/R$ and the transition from unipolar to bipolar reflectivity transient.

To analyze the polarity change of $\Delta R_L/R$ with temperature in more detail, we divide the thermal expansion of MnSi in its nonmagnetic and magnetic contributions. The first contribution is due to thermal expansion caused by the excitation of conduction electrons as well as phonons and the latter contribution is due to the magnetovolume effect. To that end, we use the method proposed in Ref. [17]. In this approach, it is assumed that the nonmagnetic coefficient of linear thermal expansion is $\alpha_{nm} = k_e T + k_p T^3$ and not dependent on the magnetic field. This is because thermal expansion due to the excitation of conduction electrons and phonons are proportional to T and T^3 , respectively, and are not affected by magnetic field changes. We extract k_e and k_p by a least square fit to α . Further, we subtract $k_e T + k_p T^3$ from α to obtain the magnetic coefficient of linear thermal expansion α_m . In Figs. 4(a) and 4(b), α_m and α_{nm} are shown exemplarily for 0 T as a function of temperature and at 10 K as a function of the magnetic field, respectively. As known from literature [17], the negative α_m dominates α for $T < T_c$, peaks at T_c and is zero for $T \gg T_c$. Further, α_m and thus

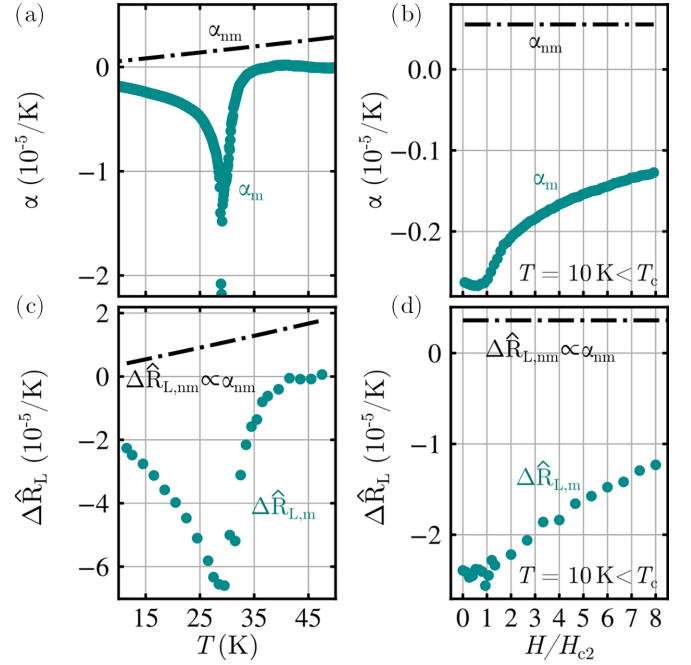


FIG. 4. (a) and (b) Magnetic (solid turquoise line) and nonmagnetic (dashed black line) coefficient of linear thermal expansion of MnSi at 0 T as a function of temperature (a) and at 10 K as a function of magnetic field (b). (c) and (d) Temperature and magnetic field dependence of the magnetic (solid turquoise line) and nonmagnetic (dashed black line) contributions to the lattice transient reflectivity at 0 T (c) and 10 K (d), respectively.

magnetovolume effect are the reason for the pronounced magnetic field dependence of α .

Using the analysis of α , we separate the magnetic $\Delta\hat{R}_{L,m}$ and non-magnetic $\Delta\hat{R}_{L,nm}$ contribution to the lattice transient reflectivity. Thereby, we assume that $\Delta\hat{R}_{L,nm}$ is proportional to α_{nm} . Further, by subtracting $\Delta\hat{R}_{L,nm}$ from $\Delta\hat{R}_L$ we extract the magnetic contribution to the lattice transient reflectivity $\Delta\hat{R}_{L,m}$, which is caused by thermal expansion due to the magnetovolume effect. $\Delta\hat{R}_{L,m}$ and $\Delta\hat{R}_{L,nm}$ are shown in Figs. 4(c) and 4(d) as a function of temperature and magnetic field, respectively. The lattice transient reflectivity is dominated by the negative $\Delta\hat{R}_{L,m}$ at low temperatures, while at $T \gg T_c$ the positive $\Delta\hat{R}_{L,nm}$ determines the lattice transient reflectivity. Thus, the bipolar reflectivity transient of Fig. 2, which we associated with a negative $\Delta R_L/R$ in Fig. 3, is due to magnetovolume effect dominating the thermal expansion below and in proximity to T_c . Thereby, the magnetovolume effect changes the optical reflectivity in an opposite manner than the nonmagnetic thermal expansion, due to its inverse effect on the lattice. With that, this study shows that α_m and thus the magnetovolume effect must be carefully considered when interpreting the transient reflectivity of magnetic materials.

VII. CONCLUSION

In conclusion, this study explores the transient reflectivity of MnSi under femtosecond alteration of long-range magnetic order. The transient reflectivity in MnSi transforms from a

unipolar behavior in the paramagnetic phase for $T \gg T_c$ to a bipolar signal in the states exhibiting magnetic long-range order for $T < T_c$. By dividing the transient reflectivity in electron and lattice contribution, our findings explain the bipolar response by the magnetovolume effect dominating the thermal expansion of MnSi. Overall this study shows that magnetovolume effect can influence the transient reflectivity and needs to be considered for a correct estimation of the transient temperature response after femtosecond laser excitation. Our work shows that the typical framework of electron and lattice transient reflectivity is valid even when the magnetovolume effect dominates the thermal expansion. This paves the way to study the time constants of the magnetovolume effect by transient reflectivity measurements, which might give further insights into the dynamics of magnetoelastic coupling.

All data needed to evaluate the conclusions of the paper are present in the paper and the Supplemental Material.

ACKNOWLEDGMENTS

We wish to thank M. Jaime for support and stimulating discussions. This work was supported by the

European Metrology Research Programme (EMRP) and EMRP participating countries under the European Metrology Programme for Innovation and Research (EMPIR) Project No. 17FUN08-TOPS Metrology for topological spin structures. In part, this study has been funded by the Deutsche Forschungsgemeinschaft (DFG, German Research Foundation) under TRR80 (From Electronic Correlations to Functionality, Project No. 107745057, Project E1), TRR360 (Constrained Quantum Matter, Project No. 492547816, Projects C1 and C3), SPP2137 (Skyrmionics, Project No. 403191981, Grants No. PF393/19 and No. SCHU 2250/8-1), the excellence cluster MCQST under Germany's Excellence Strategy EXC-2111 (Project No. 390814868) and EXC-2123 QuantumFrontiers (Project No. 390837967). Financial support by the European Research Council (ERC) through Advanced Grants No. 291079 (TOPFIT) and No. 788031 (ExQuiSid) is gratefully acknowledged.

M.B. and H.W.S. initiated the study. A.B. and C.P. grew the crystal. J.K. performed the experimental study under the supervision of M.B. and H.F. The data analysis was performed by J.K. All authors discussed the results. J.K. wrote the paper with comments of all authors.

The authors declare that they have no competing interests.

-
- [1] B. Koopmans, G. Malinowski, F. Dalla Longa, D. Steiauf, M. Fähnle, T. Roth, M. Cinchetti, and M. Aeschlimann, Explaining the paradoxical diversity of ultrafast laser-induced demagnetization, *Nat. Mater.* **9**, 259 (2010).
- [2] E. Beaurepaire, J.-C. Merle, A. Daunois, and J.-Y. Bigot, Ultrafast spin dynamics in ferromagnetic nickel, *Phys. Rev. Lett.* **76**, 4250 (1996).
- [3] C. D. Stanciu, F. Hansteen, A. V. Kimel, A. Kirilyuk, A. Tsukamoto, A. Itoh, and T. Rasing, All-optical magnetic recording with circularly polarized light, *Phys. Rev. Lett.* **99**, 047601 (2007).
- [4] M. van Kampen, C. Jozsa, J. T. Kohlhepp, P. LeClair, L. Lagae, W. J. M. de Jonge, and B. Koopmans, All-optical probe of coherent spin waves, *Phys. Rev. Lett.* **88**, 227201 (2002).
- [5] A. M. Kalashnikova and V. I. Kozub, Exchange scattering as the driving force for ultrafast all-optical and bias-controlled reversal in ferrimagnetic metallic structures, *Phys. Rev. B* **93**, 054424 (2016).
- [6] U. Atxitia, O. Chubykalo-Fesenko, N. Kazantseva, D. Hinzke, U. Nowak, and R. W. Chantrell, Micromagnetic modeling of laser-induced magnetization dynamics using the Landau-Lifshitz-Bloch equation, *Appl. Phys. Lett.* **91**, 232507 (2007).
- [7] P. B. Allen, Theory of thermal relaxation of electrons in metals, *Phys. Rev. Lett.* **59**, 1460 (1987).
- [8] P. Winsemius, F. van Kampen, H. Lengkeek, and C. van Went, Temperature dependence of the optical properties of Au, Ag and Cu, *J. Phys. F* **6**, 1583 (1976).
- [9] K. Liu, X. Shi, F. Angeles, R. Mohan, J. Gorchon, S. Coh, and R. B. Wilson, Differentiating contributions of electrons and phonons to the thermoreflectance spectra of gold, *Phys. Rev. Mater.* **5**, 106001 (2021).
- [10] J. Hohlfeld, S.-S. Wellershoff, J. Güdde, U. Conrad, V. Jähnke, and E. Matthias, Electron and lattice dynamics following optical excitation of metals, *Chem. Phys.* **251**, 237 (2000).
- [11] R. W. Schoenlein, W. Z. Lin, J. G. Fujimoto, and G. L. Eesley, Femtosecond studies of nonequilibrium electronic processes in metals, *Phys. Rev. Lett.* **58**, 1680 (1987).
- [12] M. Djordjevic, M. Lüttich, P. Moschkau, P. Guderian, T. Kampfrath, R. G. Ulbrich, M. Münzenberg, W. Felsch, and J. S. Moodera, Comprehensive view on ultrafast dynamics of ferromagnetic films, *Phys. Status Solidi (c)* **3**, 1347 (2006).
- [13] G. L. Eesley, Observation of nonequilibrium electron heating in copper, *Phys. Rev. Lett.* **51**, 2140 (1983).
- [14] S. I. Anisimov, B. L. Kapeliovich, and T. L. Perel'man, Electron emission from metal surfaces exposed to ultrashort laser pulses, *Zh. Eksp. Teor. Fiz* **66**, 375 (1974) [*Sov. Phys.-JETP* **39**, 375 (1974)].
- [15] J. P. Joule, On the effects of magnetism upon the dimensions of iron and steel bars, *Philosophical Magazine* **30**, 76 (1847).
- [16] L. McKeenan and P. Cioffi, Magnetostriction in permalloy, *Phys. Rev.* **28**, 146 (1926).
- [17] M. Matsunaga, Y. Ishikawa, and T. Nakajima, Magneto-volume effect in the weak itinerant ferromagnet MnSi, *J. Phys. Soc. Jpn.* **51**, 1153 (1982).
- [18] E. Fawcett, J. Maita, and J. Wernick, Magnetoelastic and thermal properties of MnSi, *Int. J. Magn.* **1**, 29 (1970).
- [19] S. M. Stishov, A. E. Petrova, S. Khasanov, G. K. Panova, A. A. Shikov, J. C. Lashley, D. Wu, and T. A. Lograsso, Magnetic phase transition in the itinerant helimagnet MnSi: Thermodynamic and transport properties, *Phys. Rev. B* **76**, 052405 (2007).
- [20] A. E. Petrova and S. M. Stishov, Thermal expansion and magnetovolume studies of the itinerant helical magnet MnSi, *Phys. Rev. B* **94**, 020410(R) (2016).
- [21] C. v. Korff Schmising, A. Harpoeth, N. Zhavoronkov, Z. Ansari, C. Aku-Leh, M. Woerner, T. Elsaesser, M. Bargheer, M. Schmidbauer, I. Vrejoiu, D. Hesse, and M. Alexe, Ultrafast magnetostriction and phonon-mediated stress in a photoexcited ferromagnet, *Phys. Rev. B* **78**, 060404(R) (2008).

- [22] A. Reid, X. Shen, P. Maldonado, T. Chase, E. Jal, P. Granitzka, K. Carva, R. Li, J. Li, L. Wu *et al.*, Beyond a phenomenological description of magnetostriction, *Nat. Commun.* **9**, 388 (2018).
- [23] K. Kubota, Transient magnetostriction in ferro- and ferromagnetic materials, *J. Phys. Chem. Solids* **36**, 1329 (1975).
- [24] S. M. Stishov, A. E. Petrova, S. Khasanov, G. K. Panova, A. A. Shikov, J. C. Lashley, D. Wu, and T. A. Lograsso, Heat capacity and thermal expansion of the itinerant helimagnet MnSi, *J. Phys.* **20**, 235222 (2008).
- [25] A. Bauer and C. Pfleiderer, Magnetic phase diagram of MnSi inferred from magnetization and ac susceptibility, *Phys. Rev. B* **85**, 214418 (2012).
- [26] S. Mühlbauer, B. Binz, F. Jonietz, C. Pfleiderer, A. Rosch, A. Neubauer, R. Georgii, and P. Böni, Skyrmion lattice in a chiral magnet, *Science* **323**, 915 (2009).
- [27] See Supplemental Material at <http://link.aps.org/supplemental/10.1103/PhysRevB.110.014415> for more information on (I) the temperature increase due to laser heating, (II) the temperature and magnetic field dependence of the transient reflectivity of MnSi, (III) the model used to fit the bipolar transient reflectivity, and (IV) the analysis of the coefficient of linear thermal expansion, which includes Ref. [34].
- [28] J. D. Koralek, D. Meier, J. P. Hinton, A. Bauer, S. A. Parameswaran, A. Vishwanath, R. Ramesh, R. W. Schoenlein, C. Pfleiderer, and J. Orenstein, Observation of coherent helimagnons and Gilbert damping in an itinerant magnet, *Phys. Rev. Lett.* **109**, 247204 (2012).
- [29] J. Kalin, S. Sievers, H. Füsler, H. W. Schumacher, M. Bieler, F. García-Sánchez, A. Bauer, and C. Pfleiderer, Optically excited spin dynamics of thermally metastable skyrmions in $\text{Fe}_{0.75}\text{Co}_{0.25}\text{Si}$, *Phys. Rev. B* **106**, 054430 (2022).
- [30] T. Schwarze, J. Waizner, M. Garst, A. Bauer, I. Stasinopoulos, H. Berger, C. Pfleiderer, and D. Grundler, Universal helimagnon and skyrmion excitations in metallic, semiconducting and insulating chiral magnets, *Nat. Mater.* **14**, 478 (2015).
- [31] We note that a distinct transient reflectivity behavior above and below the critical temperature was also documented in Ref. [28] on the chiral helimagnet $\text{Fe}_{0.8}\text{Co}_{0.2}\text{Si}$. The reflectivity measurements exhibited a transition from a rapid positive transient ($T > T_c$) to a slow negative transient ($T < T_c$). The authors did not observe a bipolar signal in the magnetically ordered states as observed in our study. Our experimental setup yielded similar reflectivity transients for $\text{Fe}_{0.75}\text{Co}_{0.25}\text{Si}$ compared to MnSi. However, the initial sudden increase in the reflectivity signal for $\text{Fe}_{0.75}\text{Co}_{0.25}\text{Si}$ was smaller compared to MnSi. This difference, combined with possible limitations in time resolution in Ref. [28], may explain why the bipolar reflectivity transient was not observed for $T < T_c$ in Ref. [28].
- [32] T. Kampfrath, R. G. Ulbrich, F. Leuenberger, M. Münzenberg, B. Sass, and W. Felsch, Ultrafast magneto-optical response of iron thin films, *Phys. Rev. B* **65**, 104429 (2002).
- [33] L. Waldecker, R. Bertoni, R. Ernstorfer, and J. Vorberger, Electron-phonon coupling and energy flow in a simple metal beyond the two-temperature approximation, *Phys. Rev. X* **6**, 021003 (2016).
- [34] A. Bauer, M. Garst, and C. Pfleiderer, Specific heat of the skyrmion lattice phase and field-induced tricritical point in MnSi, *Phys. Rev. Lett.* **110**, 177207 (2013).